MOBILITY OF BASAL DISLOCATIONS INTERACTING WITH NON BASAL DISLOCATIONS IN ZINC

Norio Nagata* and T. Vreeland, Jr.
W. M. Keck Laboratories, California Institute of Technology
Pasadena, California 91109

Introduction

Studies of the mobility of basal dislocations in zinc (1, 2) by use of a torsion stress pulsing technique (3) have shown that the maximum velocity of dislocations, V_{max}, is a linear function of applied shear stress, τ, at stresses above 10^6 dyne/cm^2 as expressed by

$$B\, V_{max} = \tau b \qquad (1)$$

where B is a drag coefficient and b is the basal Burgers vector. It has been concluded that some type of dislocation-phonon interaction is responsible for the damping of dislocation motion in an otherwise perfect crystal. Flow stress measurements have indicated a strong interaction between basal dislocations and forest dislocations (4). Hence, the scatter observed in the data of basal dislocation mobility measurements (1, 2) can be considered to be the result of interaction with non basal forest dislocations, whose density ranged between 10^2 and 10^4 cm^{-2}.

Recently, Frost and Ashby (5) analyzed the viscously damped motion of a dislocation through a regular array of discrete obstacles. Their calculations predicted that, at applied stresses higher than twice the critical stress to break through the obstacles ($\tau > 2\tau_c$), the motion of the dislocation is essentially governed by the viscous drag and not the obstacles. In the range $\tau_c < \tau < 2\tau_c$, the average dislocation velocity is influenced by both the viscous drag and the obstacles. Existence of a critical stress for dislocation motion through random arrays of obstacles has also been predicted by a statistical analysis (6), and by a computer analysis (7).

The strong influence of forest dislocations on the flow stress has been reported for close packed metals under the conditions of macroscopic deformation at high strain rates. Dorn et al. (8, 9, 10) and Kumar et al. (11) found a linear dependence of the flow stress on shear strain rate, expressed as

$$(\tau - \tau_B) = \alpha\dot{\gamma} \qquad (2)$$

where τ_B is a back stress, α is constant and $\dot{\gamma}$ is the shear strain rate. The shear strain rate $\dot{\gamma}$ can be expressed by

$$\dot{\gamma} = \rho b V \qquad (3)$$

where ρ is the mobile dislocation density and V is the average dislocation velocity so the relation between shear stress and the dislocation velocity can be written as

$$(\tau - \tau_B)b = \alpha\rho b V. \qquad (4)$$

*On leave from National Research Institute for Metals, Tokyo, Japan

Prestraining increases τ_B but not the value of α. Further, τ_B was considered a measure of the stress needed to overcome the internal stress field due to forest dislocations. Nagata and Yoshida (12), however, have shown that the strain rate dependence of the flow stress of Cu at high strain rates obeys Eq. 1, i.e. $\tau_B = 0$ in Eqs. 2 and 4. In their experiments, the dislocation density was at least two orders of magnitude lower than those of references 8 - 11.

The present investigation was undertaken to obtain quantitative information on how the forest dislocations affect the mobility of basal dislocations in zinc and to compare the results with theoretical predictions.

Specimens and Experimental Procedure

Crystals grown from 99.999% Zn were acid machined into rectangular blocks with (0001), $(01\bar{1}0)$, and $(2\bar{1}\bar{1}0)$ faces. The (0001) faces were cleaved and the blocks were annealed at 370°C for 1/2 hr. in an argon atmosphere. The density of forest dislocations at this stage varied between 10^2 and 10^3 cm^{-2}.

Additional forest dislocations were introduced by compressing the annealed specimens in the $[2\bar{1}\bar{1}0]$ direction, as indicated in Fig. 1. This produced forest dislocations with Burgers vectors $\pm (\underline{c} + \underline{a}_1)$ on $(2\bar{1}\bar{1}2)$ planes and $\pm (\underline{c} - \underline{a}_1)$ on $(\bar{2}112)$ planes. The deformed crystals were then acid machined to 12.7 mm diameter cylinders 5 to 10 mm long with [0001] axes and annealed at various temperatures for extended periods. In this manner the final density of forest dislocations, ρ_f, measured by means of an etch pit method (13), could be controlled over the range from 10^2 to 10^5 cm^{-2}.

Basal edge dislocations were introduced into each test specimen by scratching the end surface with an Al_2O_3 whisker along the three $\langle 10\bar{1}0 \rangle$ directions shown in Fig. 1.

The scratched surface of the specimen was bonded to a torsion testing machine as described in (2) and a torsion pulse was applied. Pulse durations ranged from 30 to 100 μ sec and resolved shear stresses ranged from 0 to 28.5 x 10^6 dyne/cm^2. The time between scratching and loading was less than one hour. Dislocation displacements were determined by use of the Berg-Barrett X-ray technique (14) before and after tests and velocities were obtained from knowledge of the displacements and the pulse duration. After taking Berg-Barrett pictures, the specimens were etched and forest dislocation densities around the scratches were measured.

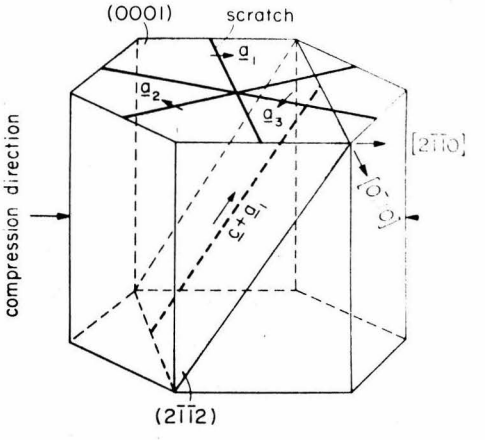

FIG. 1
Schematic diagram indicating the scratches and basal and non-basal dislocations in a test specimen.

Experimental Results

Fig. 2 shows Berg-Barrett photographs of the dislocation configurations around scratches before and after testing. Fig. 2b is an example of the edge dislocation displacements for specimens with low forest dislocation densities ($\approx 10^2$ cm^{-2}). The dislocation displacements are seen to be a linear function of radius. Since the specimen is loaded in torsion, the

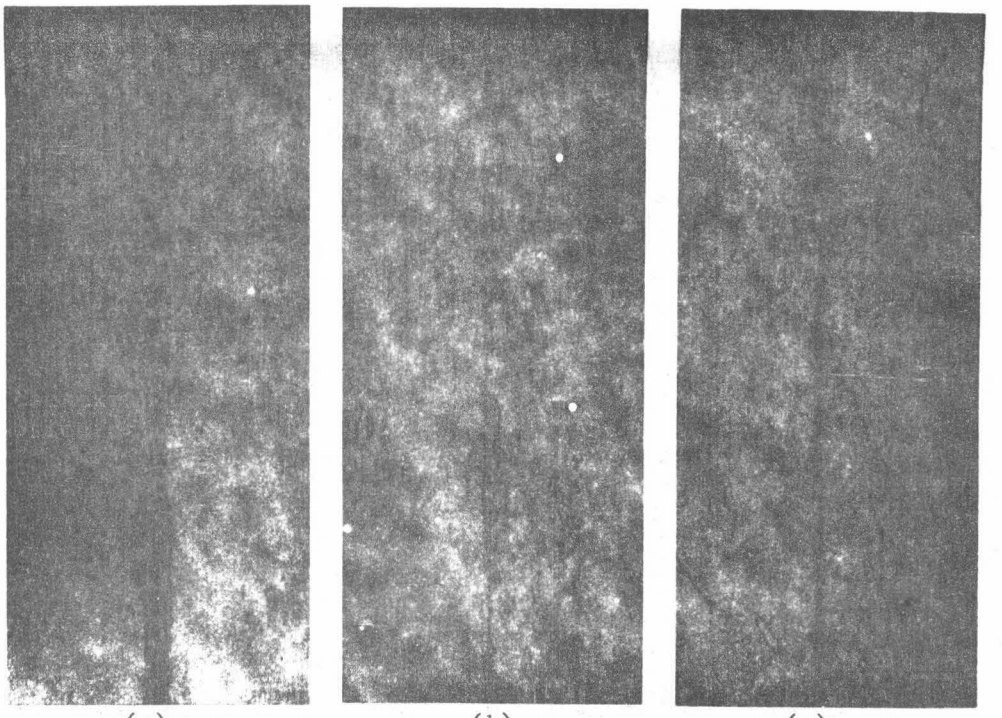

(a) (b) (c)

FIG. 2
Berg-Barrett X-ray topographs of (0001) test surfaces. (a) after scratching (b) after the torsion test (average dislocation density is about 10^2 cm^{-2}.) (c) after the torsion test (average dislocation density is 7×10^4 cm^{-2}). 27.5 X.

shear stress on a basal plane is a linear function of radius given by

$$\tau = \tau_{max} (r/R) \qquad (5)$$

where τ_{max} is the stress at the maximum radius, R, and r is the distance from the specimen center. Therefore, it is clear that the dislocation velocity is a linear function of stress. Fig. 2c is an example of dislocation displacements for specimens with high forest dislocation densities. The average forest density in this case is $7 \times 10^4 cm^{-2}$. In contrast with Fig. 2b, dislocation displacements are not linear with radius. Fig. 3 is the maximum displacement versus radius plot obtained from Fig. 2c. The envelope of the dislocation displacements is quite similar to that predicted by Frost and Ashby (5). The dislocation displacements can be divided into three distinct regions i.e., a low stress region showing no dislocation displacement, a high stress region with a linear displacement with radius and, in between, a transient region. Also Fig. 2c clearly reveals the existence of a critical shear stress for the motion of dislocations.

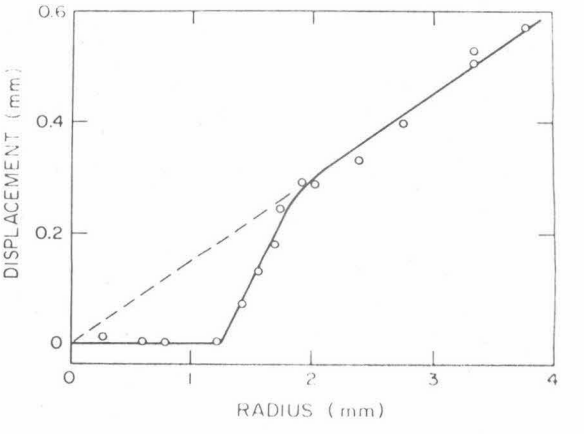

FIG. 3
Basal Dislocation displacement as a function of specimen radius.

The critical stress $\tau_{c\ exp}$ was determined from the radius at which dislocations start to move. The forest dislocation density was determined by measuring the dislocation etch pit density in a small area of the order of $10^{-4}cm^2$ where basal dislocations along each scratch just started to move. Values given in Table 1 were determined from four half scratches among six half scratches on a specimen with an average forest dislocation density of $1.9 \times 10^5 cm^{-2}$.

In the high stress region the maximum displacements are linear with radius as seen in Fig. 3. This implies that Eq. 1 is obeyed in the high stress region ($\tau_B = 0$ in Eq. 4) for forest densities up to $10^5 cm^{-2}$. The drag coefficient B for Fig. 2c turns out to be 3.1×10^{-4} dyne sec/cm^2, which is in good agreement with the value of 3.5×10^{-4} dyne sec/cm^2 previously reported (2).

Additional experiments with forest densities ranging between 10^4 and $10^5 cm^{-2}$ gave qualitatively similar results.

TABLE 1

Experimental Values of τ_c and K

Interaction	Dislocation density cm^{-2}	$\tau_{c\ exp.}$ dyne/cm^2	$K = \frac{\tau_{c\ exp.}}{Gb\sqrt{\rho_f}}$
$\underline{a}_1 + (\underline{c} \pm \underline{a}_1)$	1.8×10^5	3.6×10^6	0.82
$\underline{a}_1 + (\underline{c} \pm \underline{a}_1)$	2.0×10^5	4.4×10^6	0.94
$\underline{a}_2 + (\underline{c} \pm \underline{a}_1)$	1.8×10^5	2.5×10^6	0.57
$\underline{a}_3 + (\underline{c} \pm \underline{a}_1)$	2.0×10^5	3.1×10^6	0.66

Discussion

Critical shear stress for the motion of dislocations.

When a dislocation moves through regular arrays of discrete point obstacles, the stress required to penetrate the obstacles is given by

$$\tau_c = KG\ b/\ell \qquad (6)$$

where K is a constant ≤ 1, G is the shear modulus and ℓ is the distance between obstacles. The value of K depends on the strength of the obstacles and for strong obstacles K = 1. However, according to Kocks (6) and Foreman and Makin (7), τ_c, the critical stress for dislocations moving through random arrays of obstacles is always less than the stress in Eq. 6, where $\ell = 1/\sqrt{\rho_f}$. They found that for strong obstacles K is given as 0.84 (6) and 0.81 (7).

Experimental values of the constant K applicable to the particular intersection process were calculated using Eq. 6 with $\ell = 1/\sqrt{\rho_f}$, and is also tabulated in Table 1. The value of K for the interaction between $\underline{a}_1$ basal dislocations and $\underline{c} \pm \underline{a}_1$ non basal dislocations is between 0.8 and 0.9 in excellent agreement with the theoretical predictions for strong obstacles. This agreement implies that the interaction between basal dislocations and non-basal dislocations is quite strong as pointed out by Stofel and Wood (4). The K values

for $\underline{a}_2$ and $\underline{a}_3$ basal dislocations imply weaker interactions with the ($\underline{c} \pm \underline{a}_1$) dislocations.

The interaction $\underline{a}_1 + (\underline{c} - \underline{a}_1)$ is attractive and produces a sessile dislocation with Burgers vector $\underline{c}$ which lies on the intersection between basal and pyramidal planes. The interaction $\underline{a}_1 + (\underline{c} + \underline{a}_1)$ is repulsive, the intersection process produces a glissile jog on the basal dislocation. Theory indicates that both of these interactions should be stronger than the $\underline{a}_2$ or $\underline{a}_3$ and ($\underline{c} \pm \underline{a}_1$) interactions.

Drag Coefficient B

As stated earlier, Frost and Ashby (5) have predicted that the viscous drag should control dislocation velocity in the high stress regions even for specimens with high forest densities when the internal stress field of the forest dislocations is neglected (discrete obstacles). An example for this is the dislocation displacements in Fig. 3 which gives the value of B in good agreement with that for specimens with a dislocation density of about 10^2 cm^{-2}. This means that the dislocation travels as if in free-flight, at velocity $V = \tau b/B$, even though the dislocation cuts through a number of forest dislocations.

Preliminary results indicate that Eq. 1 may not be obeyed in the high stress region for specimens with forest dislocation densities above 10^5 cm^{-2}. This may imply that the dislocation velocity is controlled not only by the viscous drag but by an additional retarding force. Since the discrete obstacles do not influence B at $\tau > 2\tau_c$, a possible source is the varying internal elastic stress field due to forest dislocations. The mean value of the internal stress field is zero, but Li (15) has shown that the average velocity of a dislocation is decreased by such an internal stress.

References

(1) D. P. Pope, T. Vreeland, Jr. and D. S. Wood, J. Appl. Phys., 38, 4011 (1967).

(2) D. P. Pope and T. Vreeland, Jr., Phil.Mag., 20, 1163 (1969).

(3) D. P. Pope, T. Vreeland, Jr. and D. S. Wood, Rev. Scient. Instrum., 35, 1351 (1964).

(4) E. J. Stofel and D. S. Wood, Fracture of Solids, p. 521, Interscience, New York (1963).

(5) H. J. Frost and M. F. Ashby, Tech. Report No. 1 O.N.R. Contract N00014-67-A-0298-0020.

(6) U. F. Kocks, Phil. Mag., 13, 541 (1966).

(7) A. J. E. Foreman and M. J. Makin, Phil. Mag. 14, 911 (1966).

(8) W. G. Ferguson, A. Kumar and J. E. Dorn, J. Appl. Phys., 38, 1863 (1967).

(9) M. P. Victoria, C. K. H. Dharan, F. E. Hauser and J. E. Dorn, J. Appl. Phys., 41, 674 (1970).

(10) W. G. Ferguson, F. E. Hauser and J. E. Dorn, Brit. J. Appl. Phys., 18, 411 (1967).

(11) A. Kumar and R. G. Kimble, J. Appl. Phys., 40, 3475 (1969).

(12) N. Nagata and S. Yoshida, J. Japan Inst. Metals, 31, 735 (1967). (in Japanese)

(13) W. Miller, N. Nagata and T. Vreeland, Jr., to be published.

(14) A. P. L. Turner, T. Vreeland, Jr. and D. P. Pope, Acta Cryst., A24, 452 (1968).

(15) J. C. M. Li, Dislocation Dynamics, p. 87, McGraw-Hill, New York (1968).